American Mineralogist, Volume 105, pages 561–568, 2020

The new K, Pb-bearing uranyl-oxide mineral kroupaite: Crystal-chemical implications for the structures of uranyl-oxide hydroxy-hydrates

Jakub Plášil[1,*], Anthony R. Kampf[2], Travis A. Olds[3], Jiří Sejkora[4], Radek Škoda[5,†], Peter C. Burns[3,‡], and Jiří Čejka[4]

[1]Institute of Physics ASCR, v.v.i., Na Slovance 1999/2, 18221 Prague 8, Czech Republic
[2]Mineral Sciences Department, Natural History Museum of Los Angeles County, 900 Exposition Boulevard, Los Angeles, California 90007, U.S.A.
[3]Department of Civil and Environmental Engineering and Earth Sciences, University of Notre Dame, Notre Dame, Indiana 46556, U.S.A.
[4]Department of Mineralogy and Petrology, National Museum, Cirkusová 1740, Prague 9-Horní Počernice, 193 00, Czech Republic
[5]Department of Geological Sciences, Faculty of Science, Masaryk University, Kotlářská 2, 611 37, Brno, Czech Republic

Abstract

Kroupaite (IMA 2017-031), ideally $KPb_{0.5}[(UO_2)_8O_4(OH)_{10}]\cdot 10H_2O$, is a new uranyl-oxide hydroxyl-hydrate mineral found underground in the Svornost mine, Jáchymov, Czechia. Electron-probe microanalysis (WDS) provided the empirical formula $(K_{1.28}Na_{0.07})_{\Sigma 1.35}(Pb_{0.23}Cu_{0.14}Ca_{0.05}Bi_{0.03}Co_{0.02}Al_{0.01})_{\Sigma 0.48}[(UO_2)_{7.90}(SO_4)_{0.04}O_{4.04}(OH)_{10.00}]\cdot 10H_2O$, on the basis of 40 O atoms apfu. Sheets in the crystal structure of kroupaite adopt the fourmarierite anion topology, and therefore kroupaite belongs to the schoepite-family of minerals with related structures differing in the interlayer composition and arrangement, and charge of the sheets. Uptake of dangerous radionuclides (^{90}Sr or ^{135}Cs) into the structure of kroupaite and other uranyl-oxide hydroxy-hydrate is evaluated based on crystal-chemical considerations and Voronoi-Dirichlet polyhedra measures. These calculations show the importance of these phases for the safe disposal of nuclear waste.

Keywords: Kroupaite, new mineral species, uranyl-oxide hydroxy-hydrate, crystal structure, Voronoi-Dirichlet polyhedral, ^{135}Cs; ^{90}Sr; Jáchymov

Introduction

Uranium dioxide, as nuclear fuel or uraninite (Janeczek et al. 1999), UO_{2+x}, readily reacts with oxygen and water to form a fascinating family of uranyl-oxide hydroxyl-hydrates (UOHs) (Finch and Ewing 1991; Wronkiewicz et al. 1996; Plášil 2014). These occur in nature as minerals and are among the first alteration products that form during weathering of uraninite in oxidized zones of U deposits worldwide (Finch et al. 1996a, 1996b; Plášil 2018a). They are of interest in forensic studies of intercepted illicit nuclear materials as they provide insights into uranium oxide history. Several studies have focused on their structures, solubilities, and thermodynamic stabilities (Casas et al. 1997; Finch and Murakami 1999; Kubatko et al. 2006a; Klingensmith et al. 2007; Gorman-Lewis et al. 2008; Kirkegaard et al. 2019), due to their general importance in nuclear waste disposal and the environmental chemistry of uranium.

The onset of oxidation and hydration of uranium oxide often yields phases consisting of electroneutral sheets of uranyl pentagonal bipyramids with substantial H_2O in the interlayer region, and typically little, if any, additional metal cations (Burns 2005; Krivovichev and Plášil 2013; Lussier et al. 2016; Plášil 2018a). In some cases, uranium oxide hydrates containing mixtures of U(IV), U(V), or U(VI) oxidation states occur as well. Continued alteration of uranium oxide, alteration in more chemically diverse aqueous fluids, and alteration of geologically old uranium oxide that contains substantial radiogenic lead result in formation of uranyl-oxide hydroxy-hydrates with anionic sheets of uranyl polyhedra charge-balanced by cations in the interstitial regions of the structures.

Here we describe the new mineral kroupaite that was found underground in the Svornost (formerly "Einigkeit" in German) mine in Jáchymov, Western Bohemia, Czechia. Details of the mineralogy, geology, and history of the Jáchymov ore district can be found elsewhere (Ondruš et al. 2003; Hloušek et al. 2014). The specimens studied originate from the Jan Evangelista vein at the Daniel level of the Svornost mine. Associated minerals include fourmarierite, Na-rich metaschoepite, uranopilite, liebigite, ewingite, and gypsum. The new mineral and its assemblage are of supergene origin associated with oxidation-hydration alteration of uraninite in old mine workings. The name honors mining engineer Gustav Kroupa (1857–1935), who was employed by the state mines in Jáchymov beginning in 1886, and who as head of the mining district, approved shipment of 10 tons of leachate obtained from processing pitchblende ore to Marie-Curie Sklodowska and Pierre Curie in 1898. They went on to isolate three grams of the new substance radium chloride, and subsequently the new element radium. The Commission on New Minerals, Nomenclature and Classification of the International Mineralogical Association (IMA) approved the new mineral and name (IMA 2017-031). The description is based upon the holotype specimen deposited in the mineralogical collection of the National Museum in Prague (catalog number no. P1P 16/2017).

* E-mail: plasil@fzu.cz. Orcid 0000-0001-6627-5742.
† Orcid 0000-0001-6097-4294.
‡ Orcid 0000-0002-2319-9628.

0003-004X/20/0004–561$05.00/DOI: https://doi.org/10.2138/am-2020-7311

Crystals used in this study are deposited in the Natural History Museum of Los Angeles County (catalog number 66572).

Physical and optical properties

Kroupaite forms as radial aggregates of thick platy, orange-yellow crystals up to 1 mm in diameter (Fig. 1) growing in interstices of gypsum crystals. Tablets are flattened on {100}, with the prominent crystal forms {100}, {013}, and {021} (Fig. 2). Crystals are brittle with at least one cleavage, perfect on {100} and uneven fracture. Crystals are translucent with vitreous luster, have light yellow streak, and are non-fluorescent under long-wave and short-wave ultraviolet radiation. The Mohs hardness is approximately 2, estimated by scratch tests. The density was not measured due to the limited availability of material. The calculated density is 5.058 g/cm^3 based on the empirical formula. Kroupaite is readily soluble in dilute HCl, with no effervescence.

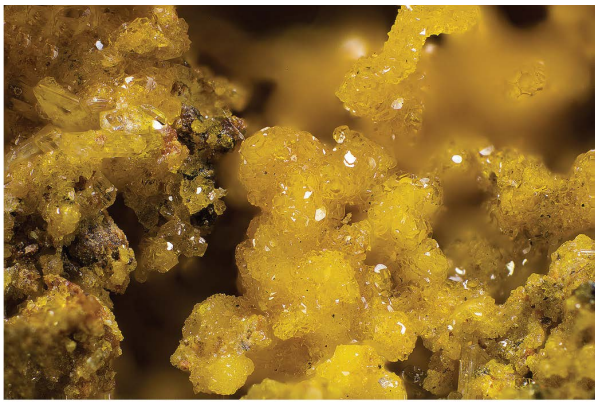

Figure 1. Orange yellow aggregates of kroupaite on the surface of strongly altered uraninite. Horizontal field of view is 2.5 mm (photo P. Škácha). (Color online.)

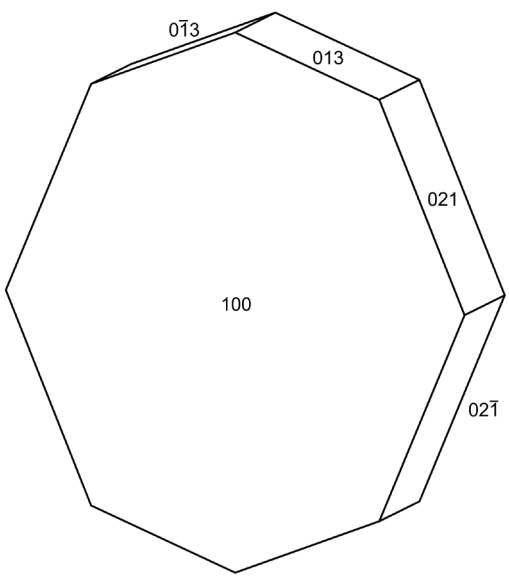

Figure 2. Crystal drawing of kroupaite in clinographic projection.

Kroupaite is optically biaxial (–), with α = 1.691(2), β = 1.752(2), γ = 1.768(2) (measured with white light). The 2*V* is 53(1)°, measured directly by conoscopic observation on a spindle stage; the calculated 2*V* is 52.7°. Dispersion is strong, *r* > *v*. The mineral is pleochroic with *X* colorless, *Y* yellow, and *Z* yellow; *X* < *Y* ≈ *Z*. The optical orientation is *X* = **a**, *Y* = **c**, *Z* = **b**. The Gladstone-Dale compatibility (Mandarino 2007), $1 - (K_p/K_c)$, is –0.018 (superior) for the empirical formula.

Raman spectroscopy

A Raman spectrum was collected in the range 4500–12 cm^{-1} using a DXR dispersive Raman Spectrometer (Thermo-Scientific) mounted on a confocal Olympus microscope. The Raman signal was excited by a green 532 nm diode-pumped solid-state laser and was collected by a CCD detector. The experimental parameters were: 50× objective, 10 s exposure time, 100 exposures, 400 lines/mm grating, 50 µm pinhole spectrograph aperture, and 1 mW laser power level. The instrument was set up by a software-controlled calibration procedure using multiple neon emission lines (wavelength calibration), multiple polystyrene Raman bands (laser frequency calibration), and standardized white-light sources (intensity calibration). Spectral manipulations as well as band-fitting were performed using the Omnic 9 software (Thermo-Scientific).

In the Raman spectrum of kroupaite (Fig. 3a) a weak broad band at 3487 cm^{-1} is assigned to the ν O–H stretching vibrations of hydroxyl and molecular H_2O H-bonded into the structure. The approximate bond-lengths of H-bonds (H···*Acceptor*) lie in the range 1.8–2.0 Å (Libowitzky 1999). The strong band centered at 833 cm^{-1}, with a shoulder at 812 cm^{-1} (Fig. 3b), is attributed to the ν_1 symmetric stretching vibration of uranyl U–O. The splitting of the ν_1 of $(UO_2)^{2+}$ is concomitant with four unique U sites observed in the crystal structure. Based on recent theoretical and experimental studies (Colmenero et al. 2018; Kirkegaard et al. 2019), the assignment of the vibration bands directly to ν_1 $(UO_2)^{2+}$ is not straightforward: the component bands comprise both symmetric stretching ν_1 $(UO_2)^{2+}$ and δ (U–OH), as well as libration vibration of (H_2O). Nevertheless, using an empirical relationship to derive the approximate U–O bond lengths from the band positions assigned to the $(UO_2)^{2+}$ stretching vibrations gives ~1.78 Å (833 cm^{-1}) and ~1.80 Å (812 cm^{-1}) (Fig. 3b). These values are in line with U–O bond-lengths obtained from the crystal structure data (see Supplemental[1] Table S1). There is a series of weak bands in the 580–280 cm^{-1} range (570, 542, 500, 450, 400, 328, and 298 cm^{-1}). Those at 570–500 cm^{-1} are attributable to librations of H_2O. Those at 450–328 cm^{-1} can be assigned to δ (O–U–O_{eq}) vibrations. According to a theoretical study of schoepite (Colmenero et al. 2018, 2020), these bands also have a significant contribution of the ν (U–O_{eq}), δ (U–OH), and libration of H_2O. The band at 298 cm^{-1} is attributed to ν_2 (δ) $(UO_2)^{2+}$, but there may be contributions from δ (O–U–O_{eq}), δ (U–OH), and water librations. Remaining bands located below 200 cm^{-1} (190, 155, 116, 63, and 40 cm^{-1}) are assigned to molecular deformations and lattice modes.

Chemical analysis

Kroupaite was analyzed by electron microprobe using a Cameca SX100 electron microprobe (Masaryk University, Brno)

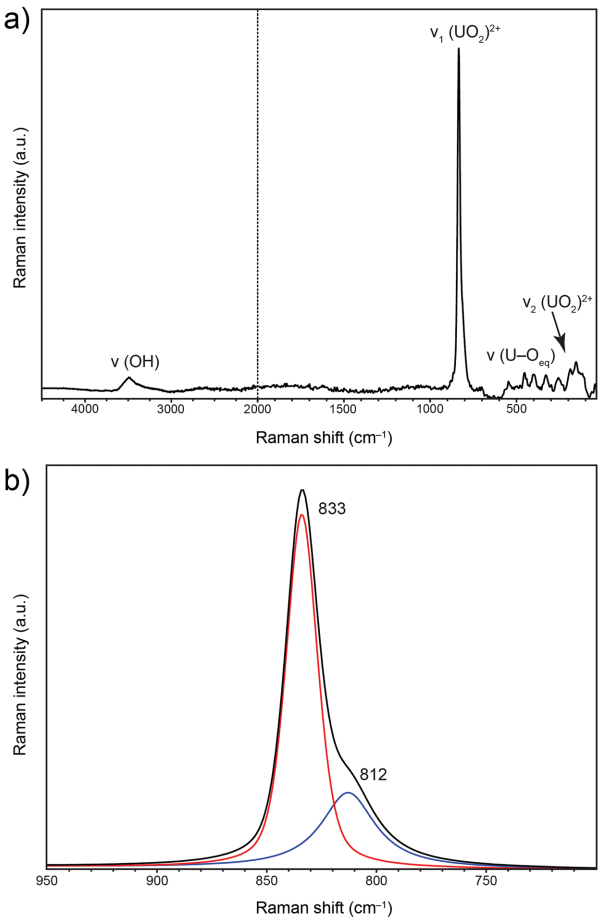

FIGURE 3. (**a**) Raman spectrum of kroupaite in the full range of 4500–12 cm^{-1} (split at 2000 cm^{-1}). (**b**) Band decomposition in the Raman spectrum of kroupaite for ν_1 $(UO_2)^{2+}$ in the region from 950–700 cm^{-1}. (Color online.)

TABLE 1. Analytical data for kroupaite (in wt%), average of six analyses

Constituent	Mean	Range	St.dev.	Probe standard	Normalized
Na_2O	0.08	0.00–0.20	0.08	albite	0.08
K_2O	2.14	1.99–2.32	0.10	sanidine	2.25
CaO	0.10	0.08–0.14	0.03	fluorapatite	0.10
PbO	1.84	1.64–2.46	0.31	vanadinite	1.93
CuO	0.41	0.00–0.72	0.28	lammerite	0.43
CoO	0.05	0.00–0.33	0.12	Co metal	0.05
Al_2O_3	0.02	0.00–0.12	0.04	sanidine	0.02
Bi_2O_3	0.25	0.00–0.51	0.19	Bi metal	0.26
UO_3	80.67	78.80–82.24	1.15	uranophane	84.64
SO_3	0.11	0.00–0.38	0.18	$SrSO_4$	0.12
H_2O[a]	9.65				10.12
Total	95.23				100.00

[a] Calculated as determined from the structure.

operating in wavelength-dispersive spectroscopy mode using an accelerating voltage of 15 kV, beam current of 4 nA, and a 10–15 μm beam diameter. Concentrations of elements other than those reported in Supplemental[1] Table S2 were below detection limits (ca. 0.03–0.10 wt%). The low analytical totals are due to an uneven surface and the porosity of the polished section; therefore, we also report normalized data (column "Norm." in Table 1). A matrix correction was applied to the data using the "*PAP*" software (Pouchou and Pichoir 1991). The H_2O content was calculated by stoichiometry (obtained from the structure); the paucity of pure material precluded a direct determination of the H_2O content. The empirical formula calculated on the basis of 40 O atoms per formula unit is: $(K_{1.28}Na_{0.07})_{\Sigma 1.35}(Pb_{0.23}Cu_{0.14}Ca_{0.05}Bi_{0.03}Co_{0.02}Al_{0.01})_{\Sigma 0.48}[(UO_2)_{7.90}(SO_4)_{0.04}O_{4.04}(OH)_{10.00}]\cdot 10H_2O$. The ideal formula is $KPb_{0.5}[(UO_2)_8O_4(OH)_{10}]\cdot 10H_2O$, which requires: K_2O 1.73, PbO 4.11, UO_3 84.21, H_2O 9.95, total 100 wt%.

X-ray crystallography and structure determination

Powder X-ray diffraction data were collected using a Rigaku R-Axis Rapid II curved imaging plate microdiffractometer with monochromated Mo*K*α radiation. A Gandolfi-like motion on the φ and ω axes was used to randomize the sample. Observed *d*-values and intensities were derived by profile fitting using the JADE 2010 software (Materials Data, Inc.). Data are given in Supplemental[1] Table S1. Unit-cell parameters refined from the powder data using JADE 2010 with whole pattern fitting are: a = 14.781(7), b = 14.095(6), c = 16.719(7) Å, V = 3583(3) Å^3, Z = 4 (space group: *Pbca*).

Single-crystal X-ray diffraction data were collected at room temperature on a Rigaku SuperNova diffractometer equipped with a microfocus X-ray source (Mo*K*α, λ = 0.71073 Å) and an Atlas S2 CCD detector. The crystal, 0.07 × 0.06 × 0.03 mm large, was mounted on a cut microloop. The raw data reduction was done using CrysAlis software (Rigaku 2019). An absorption correction combining a Gaussian correction and an empirical scaling was applied to the data using the Jana2006 software (Petříček et al. 2014). The structure was solved with SHELXT using charge-flipping (Sheldrick 2015). Full-matrix least-squares refinement of the structure against F^2 was performed with Jana2006 (Petříček et al. 2014); the structure has been refined to R = 0.0447 for 2587 unique observed reflections. The crystallographic data can be found in the original CIF (as supplementary file[1]); selected interatomic distances and results of the bond-valence analysis are given in Tables 2 and 3, respectively.

DESCRIPTION OF THE STRUCTURE

Kroupaite crystallizes in orthorhombic space group *Pbca* and its structure (Fig. 4) contains 4 U sites, 1 K site, 1 Pb site, and 19 O sites. Each U site is coordinated by seven ligands (Table 2), forming pentagonal bipyramids, where the apices of each bipyramid are comprised of strongly bonded O atoms, forming the approximately linear uranyl ion, UO_2^{2+}. In the equatorial plane, each uranyl ion is bonded to five ligands, either O or OH^- (Table 3), and the polyhedra polymerize by sharing edges and equatorial vertices (Fig. 4) into the well-known fourmarierite anion sheet topology (Fig. 5) (Burns 2005; Krivovichev and Plášil 2013; Lussier et al. 2016). In the interlayer, there are two independent cation sites that are occupied by K^+ and Pb^{2+}. Both sites have occupancies lower than unity. Additionally, there are four O sites (O15, O16, O18, O19) in the interlayer corresponding to H_2O molecules (Table 3) that were identified based on the bond-valence sums incident upon the corresponding O atoms. The K atom is [7]-fold coordinated (to 3.3 Å) and binds to five distinct O_{Ur} (Ur = uranyl) atoms. Site-scattering refinement revealed that the site is partially occupied (~0.47/0.5). The Pb site is [9]-fold

Table 2. Selected interatomic distances (Å) for kroupaite

U1-O2	1.805(10)	U2-O11	1.789(11)	U3-O4	1.765(10)
U1-O7	1.799(11)	U2-O14	1.799(12)	U3-O8	1.800(10)
U1-O1^{i}	2.231(9)	U2-O1	2.222(8)	U3-O6	2.413(9)
U1-O6	2.693(10)	U2-O10^{iii}	2.548(9)	U3-O9	2.451(9)
U1-O10^{ii}	2.460(8)	U2-O12^{iii}	2.428(10)	U3-O11	2.533(9)
U1-O13	2.254(8)	U2-O18^{ii}	2.312(9)	U3-O12	2.224(9)
U1-O22	2.434(9)	U2-O22	2.445(9)	U3-O16	2.313(9)
<*U1-O$_{Ur}$*>	1.80	<*U2-O$_{Ur}$*>	1.79	<*U3-O$_{Ur}$*>	1.78
<*U1-O$_{eq}$*>	2.41	<*U2-O$_{eq}$*>	2.39	<*U3-O$_{eq}$*>	2.39
U4-O3	1.791(12)	Pb1-O4^{iii}	2.971(11)	K1-O4^{vii}	3.201(18)
U4-O5	1.797(10)	Pb1-O5^{v}	2.804(11)	K1-O6^{vii}	2.902(18)
U4-O1	2.252(8)	Pb1-O7^{v}	3.025(11)	K1-O8^{xi}	3.201(18)
U4-O6^{iv}	2.410(9)	Pb1-O7^{iv}	3.102(11)	K1-O15	2.86(2)
U4-O11	2.471(10)	Pb1-O8^{v}	2.803(11)	K1-O16^{xi}	3.28(2)
U4-O12	2.253(9)	Pb1-O10	2.732(11)	K1-O17	2.86(2)
U4-O19	2.538(9)	Pb1-O14	2.462(14)	K1-O18	2.69(3)
<*U4-O$_{Ur}$*>	1.79	Pb1-O14^{vi}	3.036(14)	<*K1-O*>	3.00
<*U4-O$_{eq}$*>	2.39	Pb1-O18^{vii}	3.006(16)		
		<*Pb1-O*>	2.88		

Note: Symmetry codes: (i) –*x*+3/2, *y*–1/2, *z*; (ii) –*x*+3/2, –*y*+1, *z*–1/2; (iii) *x*, –*y*+3/2, *z*–1/2; (iv) –*x*+3/2, *y*+1/2, *z*; (v) *x*–1/2, –*y*+3/2, –*z*+1; (vi) –*x*+1, –*y*+2, –*z*+1; (vii) –*x*+1, –*y*+1, –*z*+1; (viii) –*x*+1, *y*+1/2, –*z*+3/2; (ix) *x*, –*y*+3/2, *z*+1/2; (x) *x*+1/2, –*y*+3/2, –*z*+1; (xi) *x*+1/2, *y*, –*z*+3/2; (xii) –*x*+3/2, –*y*+1, *z*+1/2.

coordinated (to 3.3 Å); six of the ligands are O_{Ur} atoms from adjacent structural sheets, with three from each sheet, and thus the Pb cations directly bridge between sheets. There are dimers of Pb polyhedra; one Pb-polyhedron is linked to its symmetrical equivalent through the pair of symmetrically related O16(H_2O) atoms to form $Pb_2O(O_{Ur})_{10}(H_2O)_3$ dimers.

According to the bond-valence analysis and site-scattering refinement, the formula, assuming full metal-cation site occupancy for K (0.94 K from the site-scattering refinement) and 0.5 Pb (0.44 from refinement) and full occupancies of the O(H_2O) sites, is $KPb_{0.5}[(UO_2)_8O_4(OH)_{10}]\cdot 8H_2O$, $Z = 4$, although the H_2O content is likely somewhat lower.

Relationship to other UOH minerals and compounds

The structural unit in kroupaite is the well-known fourmarierite-type sheet, which accommodates various combinations of OH^- and O in uranyl minerals, and thus has variable charge. Electroneutral sheets with composition $[(UO_2)_4O(OH)_6]$ occur in schoepite and metaschoepite (Weller et al. 2000; Plášil 2018b), whereas anionic sheets with composition $[(UO_2)_4O_2(OH)_5]^-$ occur in synthetic Na-bearing metaschoepite (Klingensmith et al. 2007) and leesite (Olds et al. 2018), and those with composition $[(UO_2)_4O_3(OH)_4]^{2-}$ occur in fourmarierite (Li and Burns 2000a).

Lead cations in the structure of kroupaite occupy the same site as Pb^{2+} in fourmarierite, but surprisingly, also the same site as K^+ in leesite (Fig. 5). In the structure of kroupaite, K atoms

Table 3. The bond-valence analysis for krouapite[a]

	U1	U2	U3	U4	Pb1[b]	K1[b]	ΣBV_{anions}	Assignment
O1	0.68	0.69		0.65			2.01	O
O2	1.66						1.66	O
O3				1.71			1.71	O
O4			1.81		0.12	0.06	1.99	O
O5				1.69	0.17		1.87	O
O6	0.25		0.46	0.46		0.12	1.29	OH
O7	1.69				0.19		1.88	O
O8			1.68		0.17	0.06	1.91	O
O9	0.42	0.35	0.42				1.19	OH
O10		1.72			0.21		1.93	O
O11		0.45	0.36	0.41			1.21	OH
O12	0.64		0.69	0.65			1.98	O
O13		1.69					1.69	O
O14					0.48		0.48	H_2O
O15						0.13	0.13	H_2O
O16		0.57	0.57			0.05	1.18	OH
O17						0.13	0.13	H_2O
O18					0.11	0.20	0.31	H_2O
O19	0.44	0.43		0.35			1.22	OH
$\Sigma BV_{cations}$	5.78	5.89	5.99	5.92	1.46	0.73		

Note: ΣBV = sum of the bond-valences; bond-valence parameters were taken from Gagné and Hawthorne (2015) and from Burns et al. (1997).
[a] All values are in valence units (v.u.).
[b] Site with a reduced occupancy.

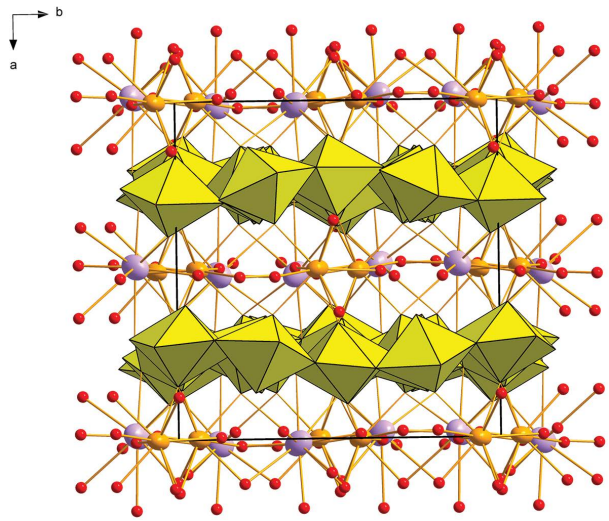

Figure 4. Crystal structure of kroupaite viewed down [001]. The uranyl-oxide hydroxide sheets (in yellow) alternate with the interlayer containing water oxygen (red), potassium (lavender), and lead (orange). Unit-cell edges are outlined by black-solid lines. (Color online.)

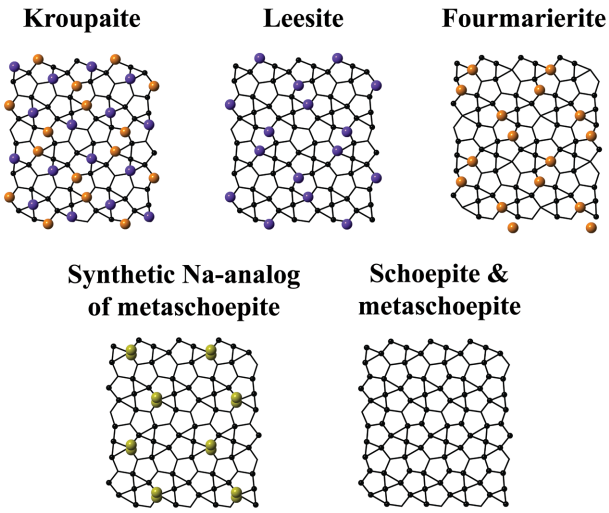

Figure 5. Comparative view of the anion sheet topologies and OH^- distributions for uranyl-oxide hydroxide-hydrate minerals with the fourmarierite topology. Black circles highlight vertices containing OH^-, and bare vertices represent O^{2-}. Orange spheres represent Pb^{2+}, blue K^+, and green Na^+ atoms, respectively. Figure adapted from Klingensmith et al. (2007). (Color online.)

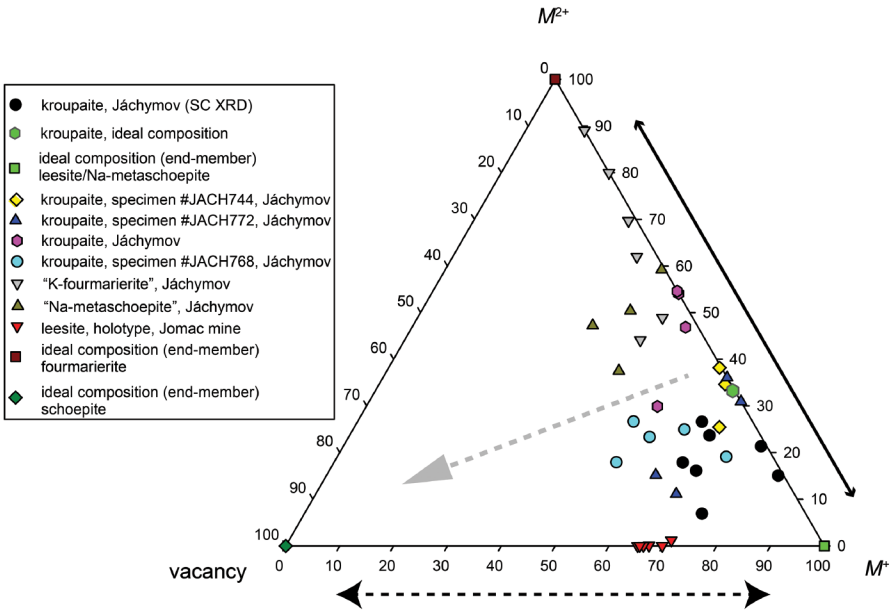

FIGURE 6. Ternary compositional plot for chemical analyses of kroupaite and related minerals. Analyses from additional set of kroupaite samples (labeled as JACH) are displayed to illustrate chemical substitutional trends. $M^{+} \leftrightarrow$ vacancy (with black dashed line): variability in composition between leesite (end-member) and schoepite; $M^{+} \leftrightarrow M^{2+}$ (black solid line): variability between leesite (end-member) and fourmarierite; the gray arrow points toward the substitution characteristic for intermediate series members and schoepite. (Color online.)

occupy the site adjacent to the dimeric Pb polyhedral units. The different behaviors of K and Pb in the structures of kroupaite and leesite are well documented by distinct substitution trends between kroupaite and fourmarierite (characteristic for the same Pb sites) and leesite (Fig. 6). The substitution in leesite should take place at the single cationic site for Pb^{2+} and K^{+}. The main structural distinction of kroupaite from leesite is a unique K^{+} site in kroupaite (Fig. 5). It appears that in the presence of Pb^{2+} with a stereoactive lone pair of electrons, K^{+} is favored at a site that provides more space and, consequently, K atoms shift to a position beneath bounding O_{Ur} atoms. The corresponding Voronoi-Dirichlet polyhedral values that characterize particular coordination environments of metal cations in the interlayers of kroupaite, leesite, fourmarierite (Fig. 7) and synthetic Na-metaschoepite are given in Supplemental[1] Table S3. Comparing Lewis acid (LA) strengths, Pb^{2+} is a much stronger acid (0.22 v.u.) than K^{+} (0.11 v.u.). Both kroupaite and leesite contain similar amounts of H_2O in their interlayers (kroupaite is slightly more hydrated) and the arrangement of $(OH)^{-}$ in the kroupaite sheet is identical to that found both in leesite and synthetic Na-metaschoepite. The consequence is that Pb adopts a site in the kroupaite structure that is more compatible with the distribution of higher bond-valence from Lewis acids to Lewis bases; in kroupaite the average Pb^{2+}–O bond-strength is 0.16 v.u. while that of K^{+}–O is 0.10 v.u. Acceptors of the majority of bonds from Pb^{2+} in kroupaite are apical uranyl atoms within the sheets.

Uranyl-oxide hydroxy-hydrates with various interlayer cations

The interstitial complexes of uranyl-oxide hydrates incorporate various elements with distinct stereochemistry. Uranyl minerals form in complex multiphase chemical conditions arising from their geological settings (and geochemistry) and are also expected to form in complex environments such as underground repositories for long-term storage of nuclear (Maher et al. 2013; Ewing 2015).

The structures and compositions of uranyl-oxide hydrates have recently been reviewed (Plášil 2018a). Crystal structures of uranyl-oxide hydrates sometimes contain U(V) or U(IV), with U(V) observed in structures containing β-U_3O_8 (Burns and Finch 1999) and α-U_3O_8 (Plášil 2017a) types of uranyl-oxide layers. In nollmotzite, $Mg[U^{V}(U^{VI}O_2)_2O_4F_3]\cdot 4H_2O$, the β-$U_3O_8$ type of sheet contains fluorine as well as oxygen (Plášil et al. 2018).

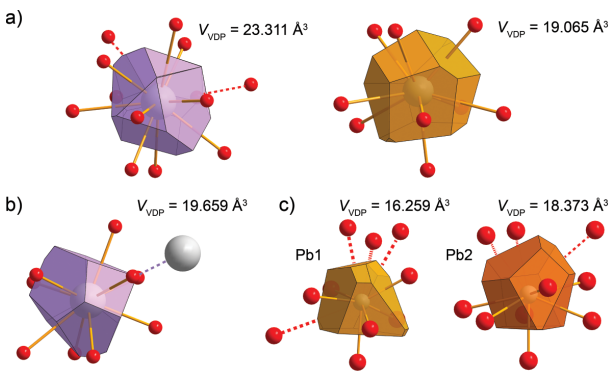

FIGURE 7. Voronoi-Dirichlet polyhedra (VDP) for interlayer cations in selected structures with corresponding VDP volumes (V_{VDP}): (**a**) kroupaite, K1 atom (lavender); Pb1 atom (orange); (**b**) leesite; K1 atom (lavender); (**c**) fourmarierite. (Color online.)

The interstitial complexes of uranyl oxide hydrates incorporate various alkali and alkaline earth cations as well as lanthanides (Hill and Burns 1999; Burns and Hill 2000a, 2000b; Cahill and Burns 2000; Zhang et al. 2018, 2019). The capacity of uranyl-oxide hydrates to accommodate cations of various Lewis-acid strengths arises in part from the heterogeneous distribution of different types of anions within the sheets: uranyl O atoms, which are somewhat undersaturated with respect to their bond-valence requirements, and OH^- groups within the uranyl-oxide layers that are bond-valence donors. These sheets readily accommodate cations of distinct charges and radii (Zhang et al. 2016), and also of different stereochemistry (Olds et al. 2017). In comparison, kamitugaite, $PbAl[(UO_2)_5(PO_4)_{2.38}(AsO_4)_{0.62}O_2(OH)_2](H_2O)_{11.5}$ (Plášil 2017b) combines divalent and trivalent cations in its interstitial complexes, and the Pb^{2+} is electron lone-pair stereoactive. The distribution of anions appears to preclude occurrence of both Pb^{2+} and Al^{3+} in the same interlayer. Thus, there are two distinct interlayers in kamitugaite, giving a large unit cell.

Voronoi-Dirichlet polyhedra (VDP) calculations (Blatov 2004) were used to evaluate and quantify bonding environments in the interlayer regions of UOHs. The VDP calculations are summarized in Supplemental[1] Table S3 and selected aspects are displayed in Figure 8. Generally, Pb^{2+} occupies sites with VDP volume (V_{VDP}) ~18 Å^3. If there is an additional cation with a larger ionic radius, as K^+ in gauthierite and kroupaite, it occupies sites with V_{VDP} >20 Å^3. In leesite, the K^+ occupies a site with V_{VDP} >19.66 Å^3 that is populated by Pb^{2+} in other uranyl-oxide-hydrate structures. The structure of gauthierite is particularly interesting as it contains four symmetrically independent partially occupied K sites. Site K2 has V_{VDP} ~27 Å^3.

TABLE 4. Ranges in charge-densities for most common topological types of UOH structural units

Topology	Charge density range (eÅ^{-3})	Range in Lewis basicity (v.u.)
α-U_3O_8	2.23×10^{-3} to 18.23×10^{-3}	0.14–0.23
β-U_3O_8	3.84×10^{-3} to 11.09×10^{-3}	0.12–0.24
Fourmarierite	2.72×10^{-3} to 6.83×10^{-3}	0.11–0.23

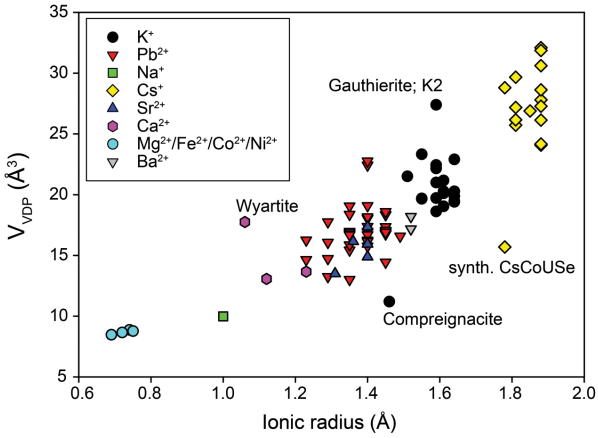

FIGURE 8. The size of cation polyhedra in the interlayers of uranyl-oxide hydroxy-hydrate structures: the volume (V_{VDP}) of Voronoi-Dirichlet polyhedra vs. the ionic radius. Outliers are labeled. (Color online.)

Potential Cs^+ and Sr^{2+} incorporation

Voronoi-Dirichlet polyhedra calculations for uranyl-oxide-hydrate structures can help in predicting incorporation of radionuclides of concern for nuclear waste disposal, such as ^{135}Cs ($t^{1/2}$ = 2.3 MY) or ^{90}Sr ($t^{1/2}$ = 28.8 Y) that are important for long-term disposal and shorter-term heat generation, respectively (Maher et al. 2013; Ewing 2015). VDP calculations are sensitive to the size of the corresponding cation and can be employed to determine characteristic volumes of corresponding cation polyhedra in uranyl-oxide-hydrate structures. Results of the analysis are given in Supplemental[1] Table S3 and Figure 8, where bonding properties of interlayer cations in most uranyl-oxide-hydrate structures based on VDP volume and corresponding ionic radii (after Shannon 1976) are listed. The ionic radii of Cs^+ and Sr^{2+} are 1.81 and 1.36 Å, respectively, and Sr^{2+} readily substitutes for Pb^{2+} and Ca^{2+}, as in agrinierite (Cahill and Burns 2000). Substitutions of Sr^{2+} for Pb^{2+} and Ca^{2+} has been documented for synthetic UOHs related to curite and becquerelite (Burns and Hill 2000a; Burns and Li 2002). Cesium is less likely to be incorporated into the interlayers of UOHs structures, although a synthetic uranyl oxide hydrate containing Cs has been reported (Hill and Burns 1999) as well as uptake of Cs^+ by a uranyl oxide hydrate during crystallization (Giammar and Hering 2004). It is plausible that Cs^+ can be incorporated in K-bearing UOHs, as the V_{VDP} of K^+ sites reaches ~24 Å^3 (with an extreme value of ~27 Å^3 in the case of K2 in gauthierite; Table 4).

Charge-density match in uranyl-oxide-hydrate structures

We used charge density calculations to identify mismatches in UOHs by modifying an approach used earlier for uranyl germanates and uranyl silicates (Li et al. 2018). The charge density ρ associated with the anionic structural units was calculated as $\rho = q_e \times Z/V$. Here q_e is the effective charge of the structural unit, which is the formal charge q_f of the structural units modified by the number of hydrogen bonds, $q_f + h \times 0.2$ (where h is the number of hydrogen atoms in the structural unit and 0.2 v.u. is the assumed bond-strength of the corresponding H bond). Z is the number of formula units in each unit cell, V is the unit-cell volume (Å^3), and ρ is then the charge density associated with the structural unit. The charge density of the interlayer complex is calculated in the same way, taking into account the formal charge of the interlayer complex modified by the H-bonds emanating from it (Supplemental[1] Table S4). The majority of UOHs structures exhibit an excess of charge density associated with the interlayer complex (Fig. 9). Exceptions are the denser (polymerized) dehydrogenated structures such as for curite and spriggite. The outlying value of the synthetic PbUOH phase (Li and Burns 2000b) is due to the density of the bond-valence acceptors within the framework as compared to the relatively simple complex occupying the channels. The high charge density of the REE^{III}-containing UOHs is associated with structural units of the α-U_3O_8 topology that are highly versatile. The variation of the charge densities for the α-U_3O_8 type sheet is the largest within the most common topological types (Table 4).

IMPLICATIONS

The new K,Pb-bearing uranyl-oxide hydroxy-hydrate kroupaite is particularly interesting due to ordering of monovalent and

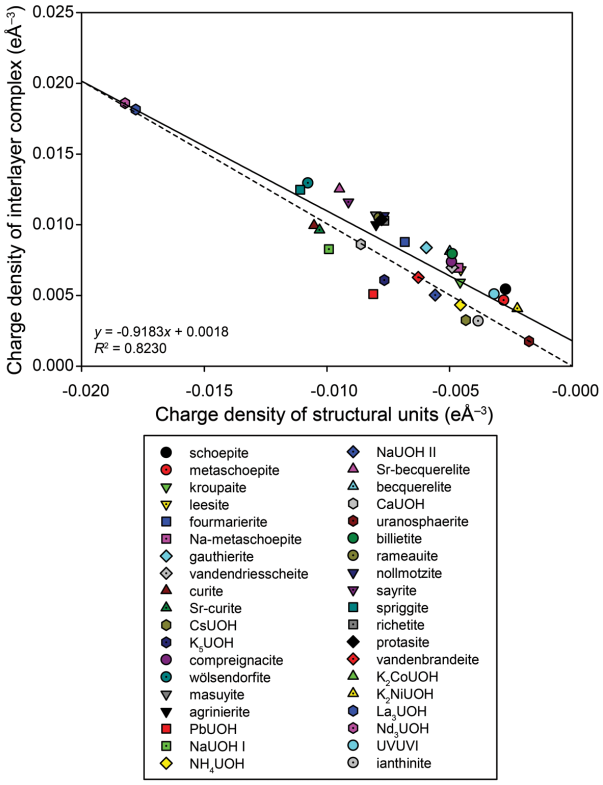

FIGURE 9. Charge-density matches in uranyl-oxide hydrate structures. The black solid line represents a linear fit to the data (equation and regression statistics given), and the dashed line represent an ideal match; $a = -1$, $b = 0$. (Color online.)

divalent cations of different stereochemistry in the interlayer region. Minerals provide unique insights into crystal chemical features that may be difficult to study via laboratory synthesis. Recent observations of natural samples, including kroupaite, leesite, and gauthierite from several localities demonstrate that uranyl-oxide-hydrate sheet anion topologies readily accommodate a range of heterovalent cations via unique configurations of their interlayers. Some uranyl-oxide-hydrate structures investigated here were found, based on analysis of their corresponding Voronoi-Dirichlet polyhedra, to be suitable for incorporation of large monovalent cations such as Cs^+.

ACKNOWLEDGMENTS AND FUNDING

Two anonymous reviewers as well as associate editor and structure editor are thanked for constructive comments, which improved the manuscript. This study was funded, in part, by the John Jago Trelawney Endowment to the Mineral Sciences Department of the Natural History Museum of Los Angeles County, by the Department of Energy, Basic Energy Sciences, Heavy Elements Program under grant number: DE-FG02-07ER15880, by the Czech Science Foundation (GACR 17-09161S to J.P., J.S., and J.Č.), and by OP VVV project (Geobarr CZ.02.1.01/0.0/0.0/16_026/0008459 to R.S.).

REFERENCES CITED

Belai, N., Frisch, M., Ilton, E.S., Ravel, B., and Cahill, C.L. (2008) Pentavalent uranium oxide via reduction of $[UO_2]^{2+}$ under hydrothermal reaction conditions. Inorganic Chemistry, 47, 10,135–10,140.

Blatov, V.A. (2004) Voronoi–dirichlet polyhedra in crystal chemistry: Theory and applications. Crystallography Reviews, 10, 249–318.

Brugger, J., Krivovichev, S.V., Berlepsh, P., Meisser, N., Ansermet, S., and Armbruster, T. (2004) Spriggite, $Pb_3[(UO_2)_6O_8(OH)_2](H_2O)_3$, a new mineral with beta-U_3O_8-type sheets: description and crystal structure. American Mineralogist, 89, 339–347.

Burns, P.C. (1997) A new uranyl-oxide-hydrate sheet in vandendriesscheite: implications for mineral paragenesis and the corrosion of spent nuclear fuel. American Mineralogist, 82, 1176–1186.

——— (1998) The structure of compreignacite, $K_2(UO_2)_3O_2(OH)_3]_2(H_2O)_7$. Canadian Mineralogist, 36, 1061–1067.

——— (1999) A new complex sheet of uranyl polyhedra in the structure of wölsendorfite. American Mineralogist, 84, 1661–1673.

——— (2005) U^{6+} minerals and inorganic compounds: insights into an expanded structural hierarchy of crystal structures. Canadian Mineralogist, 43, 1839–1894.

Burns, P.C., and Deely, K.M. (2002) Topologically novel sheet of uranyl pentagonal bipyramids in the structure of $Na[(UO_2)_4O_2(OH)_5](H_2O)_2$. Canadian Mineralogist, 40, 1579–1586.

Burns, P.C., and Finch, R.J. (1999) Wyartite: Crystallographic evidence for the first pentavalent-uranium mineral. American Mineralogist, 84, 1456–1460.

Burns, P.C., and Hanchar, J. (1999) The structure of masuyite, $Pb[(UO_2)_3O_8(OH)_2](H_2O)_3$, and its relationship to protasite. Canadian Mineralogist, 37, 1483–1491.

Burns, P.C., and Hill, F.C. (2000a) Implications of the synthesis and structure of the Sr analogue of curite. Canadian Mineralogist, 38, 175–181.

——— (2000b) A new uranyl sheet in $K_5[(UO_2)_{10}O_8(OH)_9](H_2O)$: new insights into sheet anion-topologies. Canadian Mineralogist, 38, 163–173.

Burns, P.C., and Li, Y. (2002) The structures of becquerelite and Sr-exchanged becquerelite. American Mineralogist, 87, 550–557.

Burns, P.C., Miller, M.L., and Ewing, R.C. (1996) U^{6+} minerals and inorganic phases: a comparison and hierarchy of crystal structures. Canadian Mineralogist, 34, 845–880.

Burns, P.C., Finch, R.J., Hawthorne, F.C., Miller, M.L., and Ewing, R.C. (1997) The crystal structure of ianthinite, $[U_2^{4+}(UO_2)_4O_6(OH)_4(H_2O)_4](H_2O)_5$: a possible phase for Pu^{4+} incorporation during the oxidation of spent nuclear fuel. Journal of Nuclear Materials, 249, 199–206.

Cahill, C.L., and Burns, P.C. (2000) The structure of agrinierite: a Sr-containing uranyl-oxide hydrate mineral. American Mineralogist, 85, 1294–1297.

Casas, I., Bruno, J., Cera, E., Finch, R.J., and Ewing, R.C. (1997) Characterization and dissolution behavior of a becquerelite from Shinkolobwe, Zaire. Geochimica et Cosmochimica Acta, 61, 3879–3884.

Colmenero, F., Cobos, J., and Timón, V. (2018) Periodic density functional theory study of the structure, Raman spectrum, and mechanical properties of schoepite mineral. Inorganic Chemistry, 57, 4470–4481.

Colmenero, F., Plášil, J., and Němec, I. (2020) Uranosphaerite: Crystal structure, hydrogen bonding, mechanics, infrared and Raman spectroscopy and thermodynamics. Journal of Physical Chemistry, 141, 109400.

Dao, N.Q. (1972) Structure cristalline de $Cs_2UO_2F_4H_2O$. Acta Crystallographica, B28, 2011–2015.

Ewing, R.C. (2015) Long-term storage of spent nuclear fuel. Nature Materials, 14, 252–257.

Finch, R.J., and Ewing, R.C. (1991) The corrosion of uraninite under oxidizing conditions. Journal of Nuclear Materials, 190, 133–156.

Finch, R.J., and Murakami, T. (1999) Systematics and paragenesis of uranium minerals. In P.C. Burns and R.C. Ewing, Eds., Uranium: Mineralogy, Geochemistry and the Environment, p. 38, 91–179. Reviews in Mineralogy, Mineralogical Society of America, Chantilly, Virginia.

Finch, R.J., Suksi, J., Rasilainen, K., and Ewing, R.C. (1996a) Uranium-series ages of secondary uranium minerals with applications to the long-term evolution of spent nuclear fuel. In W.M. Murphy and D.A. Knecht, Eds., Scientific Basis for Nuclear Waste Management XIX, 412, 823–830. Materials Research Society, Pittsburgh.

Finch, R.J., Cooper, M.A., Hawthorne, F.C., and Ewing, R.C. (1996b) The crystal structure of schoepite, $[(UO_2)_8O_2(OH)_{12}](H_2O)_{12}$. Canadian Mineralogist, 34, 1071–1088.

Finch, R.J., Burns, P.C., Hawthorne, F.C., and Ewing, R.C. (2006) Refinement of the crystal structure of billietite $Ba[(UO_2)_6O_4(OH)_6](H_2O)_8$. Canadian Mineralogist, 44, 1197–1205.

Gagné, O.C., and Hawthorne, F.C. (2015) Comprehensive derivation of bond-valence parameters for ion pairs involving oxygen. Acta Crystallographica, B71, 562–578.

Ghazisaeed, S., Kiefer, B., and Plášil, J. (2019) Revealing hydrogen atoms in a highly-absorbing material: an X-ray diffraction study and Torque method calculations for lead-uranyl-oxide mineral curite. RSC Advances, 9, 10058–10063.

Giammar, D.E., and Hering, J.G. (2004) Influence of dissolved sodium and cesium on uranyl-oxide hydrate solubility. Environmental Science and Technology, 38, 171–179.

Glatz, R.E., Li, Y.P., Hughes, K.A., Cahill, C.L., and Burns, P.C. (2002) Synthesis and structure of a new Ca uranyl-oxide hydrate, $Ca(UO_2)_4O_3(OH)_4)(H_2O)_2$, and its relationship to becquerelite. Canadian Mineralogist, 40, 217–224.

Gorman-Lewis, D., Fein, J.B., Burns, P.C., Szymanowski, J.E.S., and Converse, J. (2008) Solubility measurements of the uranyl-oxide hydrate phases metaschoepite, compreignacite, Na–compreignacite, becquerelite, and clarkeite. Journal of Chemical Thermodynamics, 40, 980–990.

Hawthorne, F.C. (2015) Toward theoretical mineralogy: A bond-topological approach. American Mineralogist, 100, 696–713.

Hill, F.C., and Burns, P.C. (1999) The structure of synthetic Cs uranyl hydrate and its relationship to compreignacite. Canadian Mineralogist, 37, 1283–1288.

Hloušek, J., Plášil, J., Sejkora, J., and Škácha, P. (2014) News and new minerals from Jáchymov, Czech Republic (2003–2014). Bulletin mineralogicko-petrologického oddělení Národního Muzea (Praha), 22, 155–181 (in Czech with English abstract).

Huang, J., Wang, X., and Jacobson, A.J. (2003) Hydrothermal synthesis and structures of the new open-framework uranyl silicates $Rb_4(UO_2)_2(Si_8O_{20})$ (USH-2Rb), $Rb_2(UO_2)(Si_2O_6).H_2O$ (USH-4Rb), and $A_2(UO_2)(Si_2O_6).0.5H_2O$ (USH-5A; A = Rb, Cs). Journal of Material Chemistry, 13, 191.

Janeczek, J., Ewing, R.C., Oversby, V.M., and Werme, L.O. (1999) Uraninite and UO_2 in spent nuclear fuel: a comparison. Journal of Nuclear Materials, 238, 121–130.

Kirkegaard, M.C., Niedziela, J.L., Miskowiec, A., Shields, A.E., and Anderson, B.B. (2019) Elucidation of the structure and vibrational spectroscopy of synthetic metaschoepite and its dehydration product. Inorganic Chemistry, 58, 7310–7323.

Klingensmith, A.L., Deely, K.M., Kinman, W.S., Kelly, V., and Burns, P.C. (2007) Neptunium incorporation in sodium-substituted metaschoepite. American Mineralogist, 92, 662–669.

Krivovichev, S.V., and Burns, P.C. (2001) Crystal chemistry of uranyl molybdates. IV. The structures of $M_2((UO_2)_6(MoO_4)_7(H_2O)_2)$ (M = Cs, NH_4). Canadian Mineralogist, 39, 207–214.

Krivovichev, S.V., and Plášil, J. (2013) Mineralogy and crystallography of uranium. In P.C. Burns and G.E. Sigmon, Eds., Uranium from Cradle to Grave, 43, 15–119. Mineralogical Association of Canada Short Courses.

Kubatko, K.-A., and Burns, P.C. (2006b) Cation-cation interactions in $Sr_5(UO_2)_{20}(UO_6)_2O_{16}(OH)_6(H_2O)_6$ and $Cs(UO_2)_9U_3O_{16}(OH)_5$. Inorganic Chemistry, 45, 10277–10281.

Kubatko, K.A., Helean, K., Navrotsky, A., and Burns, P.C. (2006a) Thermodynamics of uranyl minerals: Enthalpies of formation of uranyl oxide hydrates. American Mineralogist, 91, 658–666.

Li, Y., and Burns, P.C. (2000a) Investigations of crystal-chemical variability in lead uranyl-oxide hydrates. II. Fourmarierite. Canadian Mineralogist, 38, 737–749.

——— (2000b) Synthesis and crystal structure of a new Pb uranyl-oxide hydrate with a framework structure that contains channels. Canadian Mineralogist, 38, 1433–1441.

——— (2001) The structures of two sodium uranyl compounds relevant to nuclear waste disposal. Journal of Nuclear Materials, 299, 219–226.

Li, Y., Cahill, C.L., and Burns, P.C. (2001) Synthesis, structural characterization, and topological rearrangement of a novel open framework U-O material: $(NH_4)_3(H_2O)_2\{[(UO_2)_{10}O_{10}(OH)][(UO_4)(H_2O)_2]\}$. Chemistry of Materials, 13, 4026–4031.

Li, H., Langer, E.M., Kegler, P., Modolo, G., and Alekseev, E.V. (2018) Formation of open framework uranium germanates: The influence of mixed molten flux and charge density dependence in U-silicate and U-germanate families. Inorganic Chemistry, 57, 11,201–11,216.

Libowitzky, E. (1999) Correlation of O–H stretching frequencies and O–H···O hydrogen bond lengths in minerals. Monatshefte für Chemie, 130, 1047–1059.

Locock, A.J., and Burns, P.C. (2003) Structures and synthesis of framework Rb and Cs uranyl arsenates and their relationships with their phosphate analogues. Journal of Solid State Chemistry, 175, 372–379.

Lussier, A.J., Lopez, R.A.K., and Burns, P.C. (2016) A revised and expanded structure hierarchy of natural and synthetic hexavalent uranium compounds. Canadian Mineralogist, 54, 177–283.

Maher, K., Bargar, J.R., and Brown, G.E. Jr. (2013) Environmental speciation of actinides. Inorganic Chemistry, 52, 3510–3532.

Mandarino, J.A. (2007) The Gladstone–Dale compatibility of minerals and its use in selecting mineral species for further study. Canadian Mineralogist, 45, 1307–1324.

Obbade, S., Dion, C., Saadi, M., and Abraham, F. (2004) Synthesis, crystal structure and electrical characterization of $Cs_4((UO_2)_2(V_2O_7)O_2)$, a uranyl divanadate with chains of corner-sharing uranyl square bipyramids. Journal of Solid State Chemistry, 177, 1567–1574.

Olds, T.A., Plášil, J., Kampf, A.R., Škoda, R., Burns, P.C., Čejka, J., Bourgoin, V., and Boulliard, J.-C. (2017) Gauthierite, $KPb[(UO_2)_7O_5(OH)_7]\cdot 8H_2O$, a new uranyl-oxide hydroxy-hydrate mineral from Shinkolobwe with a novel uranyl-anion sheet-topology, European Journal of Mineralogy, 29, 129–141.

Olds, T., Plášil, J., Kampf, A.R., Spano, T., Haynes, P., Carlson, S.M., Burns, P.C., Simonetti, A., and Mills, O.P. (2018) Leesite, $K(H_2O)_2[(UO_2)_4O_2(OH)_5]\cdot 3H_2O$, a new K-bearing schoepite-family mineral from the Jomac mine, San Juan County, Utah, U.S.A. American Mineralogist, 103, 143–150.

Ondruš, P., Veselovský, F., Gabašová, A., Hloušek, J., Šrein, V., Vavřín, I., Skála, R., Sejkora, J., and Drábek, M. (2003) Primary minerals of the Jáchymov ore district. Journal of the Czech Geological Society, 48, 19–147.

Pagoaga, M.K., Appleman, D.E., and Stewart, J.M. (1987) Crystal structures and crystal chemistry of the uranyl-oxide hydrates becquerelite, billietite, and protasite. American Mineralogist, 72, 1230–1238.

Petříček, V., Dušek, M., and Palatinus, L. (2014) Crystallographic Computing System Jana 2006: general features. Zeitschrift für Kristallographie, 229, 345–352.

Plášil, J. (2014) Oxidation-hydration weathering of uraninite: the current state-of-knowledge. Journal of Geosciences, 59, 89–114.

——— (2017a) Crystal structure of richetite revisited: Crystallographic evidence for the presence of pentavalent uranium. American Mineralogist, 102, 1171–1175.

——— (2017b) A novel sheet topology in the structure of kamitugaite, $PbAl[(UO_2)_5(PO_4)_{2.38}(AsO_4)_{0.62}O_2(OH)_2](H_2O)_{11.5}$. Journal of Geosciences, 62, 253–260.

——— (2018a) Uranyl-oxide hydroxy-hydrate minerals: their structural complexity and evolution trends. European Journal of Mineralogy, 30, 237–251.

——— (2018b) The crystal structure of uranyl-oxide mineral schoepite, $[(UO_2)_4O(OH)_6](H_2O)_6$, revisited. Journal of Geosciences, 63, 65–73.

——— (2019) Hydrogen bonding in lead uranyl-oxide mineral sayrite. Zeitschrift für Kristallographie, 234, 733–738. DOI: 10.1515/zkri-2019-0035.

Plášil, J., Škoda, R., Čejka, J., Bourgoin, V., and Boulliard, J.-C. (2016) Crystal structure of the uranyl-oxide mineral rameauite. European Journal of Mineralogy, 28, 959–967.

Plášil, J., Kampf, A.R., Škoda, R., and Čejka, J. (2018) Nollmotzite, $Mg[U^{V}(U^{VI}O_2)_2O_4F_3]\cdot 4H_2O$, the first natural uranium oxide containing fluorine. Acta Crystallographica, B74, 362–369.

Pouchou, J.-L., and Pichoir, F. (1991) Quantitative analysis of homogeneous or stratified microvolumes applying the model "PAP." In K.F.J. Heinrich and D.E. Newbury, Eds., Electron Probe Quantitation, pp. 3l–75. Plenum Press.

Rigaku (2019) CrysAlis CCD and CrysAlis RED. Oxford Diffraction Ltd, Yarnton, Oxfordshire, U.K.

Rosenzweig, A., and Ryan, R.R. (1977) Vandenbrandeite $CuUO_2(OH)_4$. Crystal Structure Communications, 6, 53–56.

Shannon, R.D. (1976) Revised effective ionic radii and systematic studies of interatomic distances in halides and chalcogenides. Acta Crystallographica, A32, 751–767.

Sheldrick, G.M. (2015) Crystal structure refinement with SHELXL. Acta Crystallographica, C71, 3–8.

Weller, M.T., Light, M.E., and Gelbrich, T. (2000) Structure of uranium(VI) oxide dihydrate, $UO_3\cdot 2H_2O$; synthetic meta-schoepite $[(UO_2)_4O(OH)_6]\cdot 5H_2O$. Acta Crystallographica, B6, 577–583.

Wronkiewicz, D.J., Bates, J.K., Wolf, S.F., and Buck, E.C. (1996) Ten-year results from unsaturated drip tests with UO_2 at 90°C: implications for the corrosion of spent nuclear fuel. Journal of Nuclear Materials, 238, 78–95.

Wylie, E.M., and Burns, P.C. (2012) Crystal structures of six new uranyl selenate and selenite compounds and their relationship with uranyl mineral structures. Canadian Mineralogist, 50, 147–157.

Zhang, Y., Čejka, J., Lumpkin, G.R., Tran, T.T., Aharonovich, I., Karatchevtseva, I., Price, J.R., Scales, N., and Lu, K. (2016) Hydrothermal synthesis, structures and properties of two uranyl oxide-hydroxyl hydrate pahses with Co(II) or Ni(II) ions. New Journal of Chemistry, 40, 5357–5363.

Zhang, Y., Aughterson, R., Karatchevtseva, I., Kong, L., Trong Tran, T., Čejka, J., Aharonovich, I., and Lumpkin, G.R. (2018) Uranyl-oxide hydrate phases with heavy lanthanide ions: $[Ln(UO_2)_2O_3(OH)]\cdot 0.5H_2O$ (Ln = Tb, Dy, Ho and Yb). New Journal of Chemistry, 42, 12,267–13,184.

Zhang, Y., Aughterson, R., Zhang, Z., Wei, T., Lu, K., Čejka, J., and Karatchevtseva, I. (2019) Syntheses, crystal structures and spectroscopic studies of uranyl-oxide hydrate phases with La(III)/Nd(III) ions. Inorganic Chemistry, 58, 10,812–10,821.

Manuscript received October 2, 2019
Manuscript accepted November 24, 2019
Manuscript handled by G. Diego Gatta

Endnote:

[1]Deposit item AM-20-47311, Supplemental tables and CIF. Deposit items are free to all readers and found on the MSA website, via the specific issue's Table of Contents (go to http://www.minsocam.org/MSA/AmMin/TOC/2020/Apr2020_data/Apr2020_data.html).